https://doi.org/10.1016/j.ijplas.2018.01.016

Multi-Temperature Indentation Creep Tests on Nanotwinned Copper

Xu-Sheng Yang[b*], Hui-Ru Zhai[c], Hai-Hui Ruan[d], San-Qiang Shi[d,e], Tong-Yi Zhang[a†]

[a]*Shanghai University Materials Genome Institute and Shanghai Materials Genome Institute, Shanghai University, 99 Shangda Road, Shanghai 200444, China*

[b]*Department of Industrial and Systems Engineering, The Hong Kong Polytechnic University, Hung Hom, Kowloon, Hong Kong, China*

[c]*Department of Mechanical and Aerospace Engineering, The Hong Kong University of Science and Technology, Clear Water Bay, Kowloon, Hong Kong, China*

[d]*Department of Mechanical Engineering, The Hong Kong Polytechnic University, Hung Hom, Kowloon, Hong Kong, China*

[e]*Hong Kong Polytechnic University Shenzhen Research Institute, Shenzhen, China*

[*] Corresponding author. xsyang@polyu.edu.hk (X.-S Yang). Tel: +852-27666604

[†] Corresponding author. zhangty@shu.edu.cn (T.-Y Zhang). Tel & Fax: +86-21-66136172

Abstract:

The present work further develops the multi-temperature approach on load, time, and temperature-dependent deformation for indentation creep. Multi-temperature micro-indentation creep tests were carried out on nanotwinned copper (nt-Cu) at five temperatures of 22 ℃ (RT), 40 ℃, 50 ℃, 60 ℃ and 70 ℃. In analogy with stress, hardness is used to gauge the indentation creep loading level, while the indentation depth is used to characterize the indentation creep deformation and the creep strain rate is represented by the indentation depth strain rate. The multi-temperature micro-indentation creep tests generate sufficiently large experimental data, which makes the development of a novel formula for indentation creep feasible. There are few intrinsic parameters that characterize the capability of the microstructure of a material against load, time, and temperature dependent deformation and they are the strain rate sensitivity, the athermal hardness exponent, intrinsic activation energy, and activation volume. The strain rate sensitivity is determined from isothermal creep data at one temperature, while the other parameters have to be determined from multi-temperature creep data. The novel formula is validated by the experimental data of the multi-temperature indentation creep tests on the nt-Cu. The creep mechanisms of the nt-Cu are also discussed and analyzed by using the determined values of the intrinsic parameters.

Keywords: Nanotwin; Indentation creep; Creep activation parameters; Twin boundary migration; Hardness.

1. Introduction

Creep behaviors of materials under sustained load at elevated temperatures are essential to their practical applications. The rate of creep deformation is related to the types of materials, and the external conditions including load, creep time, and temperature. Based on experiments, atomistic simulations and/or theoretical models, the creep deformation behaviors and associated mechanisms of various types of materials, such as metals and alloys (Kassner and Pérez-Prado, 2004; Lee et al., 2016), polymer and composites (Jia et al., 2011; Tehrani et al., 2011), and ceramics (Gan and Tomar, 2010; Kassner et al., 2007), etc., have been extensively investigated for many years. In the conventional polycrystalline metals, the creep deformation can be accommodated by the lattice or grain boundary (GB) diffusion (Choi et al., 2013a; Coble, 1963; Fischer and Svoboda, 2011; Herring, 1950), and movements and associated consequences of interfaces, GBs and twin boundaries (TBs) (Basirat et al., 2012; Morra et al., 2009; Muñoz-Morris et al., 2009; Oberson and Ankem, 2009), and dislocation activities (Wang et al., 2011), etc.

When grain size is at the nanoscale (typically < 100 nm) in polycrystalline metals, the nanograined (ng) metals exhibit enhanced strength. However, the creep deformation is severely accelerated in the ng metals, because decreasing grain size significantly increases the volume fraction of GBs, which possess very poor thermal stability and thus provide fast diffusion path for creep deformation and failure (Sanders et al., 1997; Wang et al., 2013b; Wang et al., 2012b). The creep rate in ng metals depends greatly on the grain size, that is, the smaller the grain size is, the higher the creep rate will be (Sanders et al., 1997). Similarly, the reported uniaxial creep strains and creep strain rates in smaller Ni nano-pillars were correspondingly higher than those in Ni micro-pillars (Choi et al., 2013a) due to surface diffusion. Therefore, the weak creep resistance of ng metals is one of the bottleneck problems for their practical applications, especially at elevated

temperatures. In contrast, coherent twin boundaries (CTBs) resistance against dislocation motion is much more moderated, thereby optimizing both the strength and ductility of metals (He et al., 2016; Lu et al., 2004; Xiao et al., 2015). CTBs are not fast diffusion channels in comparison with GBs, resulting in more thermal stability of nanotwinned (nt) structures compared with the twin-free ng counterparts (Li et al., 2016; Zhang and Misra, 2012; Zheng et al., 2013). For example, the cyclic nano- and micro-indentation creep (Bezares et al., 2012) and uniaxial tensile creep experiments (Yang et al., 2016b) on nt-Cu indicate that nt structure exhibits greater creep resistance than twin-free ng-Cu, and the simulations (Jiao and Kulkarni, 2015) reveal that the creep resistance increases with decreasing TB spacing.

Nano/micro-indentation is a fast and effective technique to characterize the mechanical properties of materials at the nanometer/micrometer scales. Due to its unique feature of small size-scaled characterization, the nano/micro-indentation has been widely utilized in the mechanical characterization of various materials, especially nanomaterials, nanostructured materials, biomaterials, thin films, (Ma et al., 2012; Wang et al., 2015) etc. Within such small detected volume in nano/micro-indentation tests, the strain magnitude, the stress level, and the strain rate could be considerably high, which are hardly achieved in conventional tensile tests (Choi et al., 2013b). In normal uniaxial tensile (compression) test, the cross-head movement rate of a testing machine is pre-set and the load cell and the extension meter record, as functions of time, the load and sample displacement, respectively. Then, based on the geometry of a tested sample, load and displacement are correspondingly converted to stress and strain, and then stress rate and strain rate can be calculated. The strain rate is linked to the cross-head movement rate and a pre-set cross-head movement rate corresponds generally to a constant strain rate. In this sense, normal uniaxial tensile (compression) test is carried out under a sustained strain rate, during which the stress varies with

the deformation characterized by strain. In contrast, a sustained stress is applied on a sample in uniaxial tensile (compression) creep test and creep deformation strain is recorded with creep time. Based on the creep deformation behavior, creep deformation is usually divided into three stages of the primary (transient) stage, the secondary steady stage, and the tertiary (unstable) stage. In the primary stage, the strain rate decreases with time and reaches a steady value in the secondary stage, while in the tertiary stage, the strain rate increases until failure of the crept sample. The creep strain rate in the secondary steady stage is approximately constant independent of time, which is the most critical creep strain rate. This is because that the period of steady state creep spends, in most cases, the largest portion of the creep life, and the higher the steady creep rate is, the shorter the survival life of the crept material will be. In indentation creep tests there is a challenging issue that which parameters should be used to represent and describe the loading level and the degree of deformation. This is because the stress distribution is completely inhomogeneous inside the tested sample under an indentation load (Wang et al., 2015) and the inhomogeneous stress distribution causes inhomogeneous deformation. It is suggested that hardness might be the appropriate parameter to describe the loading level, since hardness in nanoindentation tests is defined as the averaged pressure on the project contact area. Indentation depth might be the appropriate parameter to describe the deformation, because indentation depth is the only measurable parameter in nanoindentation creep under a given indentation load (Gan and Tomar, 2011). Indentation creep is actually the inhomogeneous deformation varying with time under a given load, in which the indentation depth increases and the hardness decreases monotonically with time. Commonly, the creep deformation will eventually saturate under a given compressive indentation load (Zhang et al., 2017a).

Sharma *et al*. (Sharma et al., 2005) conducted the indentation creep tests on the iron aluminide

intermetallic (Fe-28Al-3Cr) at the temperature range of 843-963 K. The experimental results showed that the hardness decreased with creep time and the stress exponent *n* was weakly dependent on temperature, being 5.52 at 843 K and 4.53 at 963 K. The determined stress exponent of ~ 5 and the activation energy in the range of 339-341 kJ/mol (Sharma et al., 2005) were found to be consistent with the dislocation climb creep mechanism. Nanoindentation creep tests on ng Cu-based alloys at room temperature (RT) (Liu et al., 2012) exhibited that the stress exponents (ranging from 5 to 50) increased with the increase of the indentation load. Besides, it was found that the higher the temperature was, the lower the determined activation volume and stress exponent would be (Alizadeh et al., 2013; Ma et al., 2002; Ranganath and Mishra, 1996; Wang et al., 2009a). Wang *et al.* (Wang et al., 2009a) performed the indentation creep tests on the ng-Ni with grain size of 14 nm under sustained load of 1 mN at temperatures of 348 K, 398 K and 448 K, respectively. The corresponded stress exponents and activation volumes at the three temperatures were determined to be 14.81 and $3.78b^3$, 7.14 and $2.74b^3$, and 4.91 and $2.48b^3$, where *b* denoted the magnitude of Burgers vector. The calculated activation energy of 123.1 kJ/mol was remarkably close to that for the GB self-diffusion in Ni, but far less than that for lattice diffusion, indicating that the rate controlling process was meditated by GB diffusion in the ng-Ni (Wang et al., 2009a). Zhang *et al* carried out the indentation creep tests on In-617 alloy under sustained load of 200-400 mN at temperatures from RT up to 800 ℃ (Zhang et al., 2017a) and Raman spectroscopy measurements of depth sensitive stress distribution (Zhang et al., 2017b). The determined stress exponent values for the indentation creep were between 5 to 6, thereby suggesting that the creep mechanism of IN-617 at nano/micro scales was dominated by dislocation climb. The creep properties of silicon microcantilevers were in-situ investigated at temperatures of RT, 50 ℃ and 100 ℃ under uniaxial compressive stress within range of 50-100 MPa (Gan et al., 2014), showing

that the creep rate of the silicon cantilever was increased with both compressive stress and temperature.

The indentation creep behaviors depend on the experimental conditions of load, creep time, and temperature, and the micro/nanostructure of a crept material. The micro/nanostructure under the experimental conditions gives the material responses and hence yields the load, time, and temperature-dependent deformation, which can be characterized by the creep parameters of strain rate sensitivity, activation energy, activation volume, and stress exponent. The four parameters describe the material intrinsic creep behaviors and thus are micro/nanostructure related. It is desirable to let the creep intrinsic parameters be independent of the external loading conditions at least within certain ranges of the loading conditions (Gan and Tomar, 2011). To achieve this goal, Yang *et al.* (Yang et al., 2016a; Yang et al., 2016b) developed the multi-temperature approach based on the hypothesis that the temperature dependency of deformation is expressed by the Arrhenius equation, and the activation energy is independent of temperature within the temperature range and depends on applied load only. This hypothesis holds if no change in the deformation mechanism occurs within the temperature range, which should be verified by experimental results. Yang *et al.* (Yang et al., 2016a; Yang et al., 2016b) conducted tensile stress relaxation tests and tensile creep tests at various temperatures and the results validated this hypothesis. Starting from this hypothesis and based on experimental results, Yang *et al.* (Yang et al., 2016a; Yang et al., 2016b) developed a formula for load, time, and temperature-dependent deformation, which is described later in Section 2 of Theoretical Analysis. If experiments on load, time, and temperature dependent-deformation are conducted only at a temperature, we shall call this type of investigations one-temperature approach, which will be also discussed in Section 2. The goal of the present work is to build up a formula for indentation creep based on the previous work (Yang et al., 2016a; Yang

et al., 2016b) and indentation creep test results at various temperatures.

This paper is organized as follows. Firstly, Section 2 gives the theoretical analysis that illustrates the mathematically consistent multi-temperature approach for the determination of creep activation parameters and building-up the creep strain rate formula. Section 3 describes the experimental procedures of micro-indentation creep tests, which were conducted under sustained load of 100 mN at temperatures of RT, 40 ℃, 50 ℃, 60 ℃ and 70 ℃, to investigate the hardness, time, and temperature-dependent indentation creep deformation. Section 4 summarizes the experimental results of micro-indentation creep tests, which build-up the theoretical formula of Eq. (9d) to describe indentation creep deformation. The relationship between the strain rate sensitivity parameter, athermal hardness exponent and activation volume is also discussed in Section 4. Based on the determined activation parameters, Section 4 also discusses the hardness related transition of indentation creep mechanism in nt-Cu, i.e., from perfect dislocation mediated deformation to the TB migration, as the hardness decreases. Finally, concluding remarks are given in Section 5 to emphasize that the greater indentation creep resistance property of nt structure and the newly developed creep strain rate formula to describe the indentation creep deformation.

2. Theoretical Analysis

As described by the words “load, time, and temperature dependent deformation”, deformation is a function of load, time, and temperature. As described above, strain rate represents the deformation rate of crept sample under a sustained stress at a given temperature. Generally, strain rate is a function of stress, time and temperature, and in the secondary creep stage, strain rate is a function of stress and temperature merely and does not depend on time anymore. The novel formula developed in the previous work (Yang et al., 2016a; Yang et al., 2016b) is based on that strain rate depends only on stress and temperature, which is also the basis of the present theoretical analysis.

The strain rate sensitivity *m* has been used for a long time to describe the dependency of plastic strain rate, $\dot{\varepsilon}_p$, on applied stress σ at a given temperature *T* (Dieter, 1986). Its definition is given by

$$m = \left.\frac{\partial \log \sigma}{\partial \log \dot{\varepsilon}_p}\right|_T = \left.\frac{\partial \ln \sigma}{\partial \ln \dot{\varepsilon}_p}\right|_T , . \quad (1)$$

Eq. (1) indicates that the strain rate sensitivity *m* can be determined from isothermal experimental data of strain rate versus stress and thus Eq. (1) is used in the one-temperature approach and multi-temperature approach as well. As described in many literatures (Cao et al., 2012; Elmustafa and Stone, 2002; Raj and Langdon, 1989; Wang et al., 2009a; Wang et al., 2009b), experimental data curves of $\ln\sigma$ versus $\ln\dot{\varepsilon}_p$ during the tensile creep tests appear approximately linear and linearly fitting $\ln\sigma$ versus $\ln\dot{\varepsilon}_p$ determines the value of *m*. Then, integrating Eq. (1) with the linear relationship between $\ln\sigma$ and $\ln\dot{\varepsilon}_p$ gives a power-law relation of $\sigma \propto \dot{\varepsilon}_p^{\,m}$. In the one-temperature approach, it is also to take it as granted to have the power law of $\dot{\varepsilon}_p \propto \sigma^n$ in the description of strain rate dependency on stress. That is why the strain rate sensitivity *m* is believed, in the one-temperature approach, to equal to the reciprocal of conventional stress exponent 1/*n*. As indicated in Eq. (1), the strain rate sensitivity *m* is defined as the differentiation of $\ln\dot{\varepsilon}_p$ with respect to $\ln\sigma$ at a constant temperature and thus determined experimentally by carrying out creep tests at various stress levels at only one temperature. It should keep in mind that strain rate $\dot{\varepsilon}_p$ is a function of both σ and *T*. This consideration suggests that the strain rate sensitivity *m* might be related to temperature, even it is a constant at a temperature, as described below.

It is widely accepted that the temperature dependency of plastic strain rate $\dot{\varepsilon}_p$ is expressed by

the Arrhenius equation

$$\dot{\varepsilon}_p = \dot{\varepsilon}_0 \exp\left(-\frac{\Delta G}{k_B T}\right), \tag{2}$$

where $\dot{\varepsilon}_0$ is the prefactor, k_B is the Boltzmann constant, and ΔG is called the apparent (nominal) activation energy. The apparent activation energy is the real activation energy reduced by the applied stress and the activation volume *V*, as a conjugate of applied stress, is introduced to count the reduction in activation energy. Thus, we have (Zhu and Li, 2010; Zhu et al., 2007)

$$\Delta G = \Delta G_0 - \frac{\sigma}{\sqrt{3}} V, \tag{3}$$

where ΔG_0 is called the intrinsic activation energy and $1/\sqrt{3}$ is the numerical factor to convert shear stress to tensile stress. The intrinsic activation energy and the activation volume can be determined by plotting ΔG versus σ. As described above about the hypothesis, the exponential term in Eq. (2) is the only term involving temperature and stress, while the prefactor $\dot{\varepsilon}_0$ depends on applied stress only, being independent of temperature. With this hypothesis, the apparent activation energy ΔG and the prefactor $\dot{\varepsilon}_0$ are determined experimentally by plotting $\ln \dot{\varepsilon}_p$ versus reciprocal absolute temperature in the multi-temperature approach, where the data of strain rate must be obtained under a certain stress level. This means that creep tests must be carried out at various temperatures in order to experimentally determine the apparent activation energy and the prefactor. Under a certain stress level, the plot of $\ln \dot{\varepsilon}_p$ versus reciprocal absolute temperature gives a value of prefactor and a value of the apparent activation energy. Then, the values of ΔG under various stress levels allow one to calculate the activation volume by using Eq. (3) in the multi-temperature approach.

On the other hand, Eq. (2) gives the following derivation:

$$\frac{V}{\sqrt{3}} = -\frac{\partial \Delta G}{\partial \sigma} = -k_{\mathrm{B}}T\left[\frac{\partial \ln \dot{\varepsilon}_0}{\partial \sigma} - \frac{\partial \ln \dot{\varepsilon}_p}{\partial \ln \sigma}\cdot\frac{\partial \ln \sigma}{\partial \sigma}\right] = -k_{\mathrm{B}}T\left[\frac{\partial \ln \dot{\varepsilon}_0}{\partial \sigma} - \frac{1}{m\sigma}\right]. \tag{4}$$

Eq. (4) indicates that if the prefactor $\dot{\varepsilon}_0$ is stress-independent, we will have the relation between strain rate sensitivity *m* and activation volume *V* as:

$$\frac{1}{m} = \frac{\sigma V}{\sqrt{3}k_B T}. \tag{5}$$

Eq. (5) shows that the strain rate sensitivity *m* depends on temperature. In the one-temperature approach, Eq. (5) is often used to estimate the value of activation volume (Asaro and Suresh, 2005; Wei et al., 2004; Zhu et al., 2007). If one uses the power law $\dot{\varepsilon}_p \propto \sigma^{1/m}$ to describe the relationship between strain rate and stress, one cannot use Eq. (5) to estimate the value of activation volume by treating the prefactor $\dot{\varepsilon}_0$ stress-independent. The above description from Eq. (1) to Eq. (5) indicates that Eq. (5) holds only if the strain rate is expressed by the Arrhenius equation with the assumption that the prefactor is independent of stress. In this case, the strain rate cannot be expressed by the stress power law relation anymore, even experimental results show this trend of power law. In other words, if the power law relation is adopted to express the strain rate, one cannot use Eq. (5) to the value of activation volume. In one sentence, the stress power law is mathematically inconsistent with the Arrhenius equation, in which the prefactor is stress-independent. Therefore, the one-temperature approach cannot simultaneously determine both stress exponent and activation volume. This mathematic inconsistency implies that the prefactor must be stress-dependent.

As mentioned above, in the multi-temperature approach, the plot of $\ln \dot{\varepsilon}_p$ under a certain stress level versus reciprocal absolute temperature gives a value of prefactor and a value of the

apparent activation energy. Then, conducting the multi-temperature approach under various stress levels leads to many values of the prefactor and the apparent activation energy. From the values of apparent activation energy, one is able to determine the intrinsic activation energy and the activation volume with Eq. (3). The experimental results (Yang et al., 2016a; Yang et al., 2016b) exhibit also that the prefactor is stress-dependent. Usually, the stress-dependency is expressed by power law. With this consideration, Eq. (2) is further expressed by (Yang et al., 2016a; Yang et al., 2016b)

$$\dot{\varepsilon}_p(\sigma,T)=\dot{\varepsilon}_{00}\left(\frac{\sigma}{\sigma_0}\right)^{n'}\exp\left(-\frac{\Delta G_0}{k_BT}+\frac{\sigma V}{k_BT\sqrt{3}}\right), \tag{6}$$

where σ_0 is a reference stress, whose the magnitude is one and has the same unit as σ. Here, the "athermal stress exponent *n*'" is redefined to be the exponent for the prefacor in the Arrhenius equation, rather than the traditional "stress exponent *n*" for the creep strain rate in the conventional creep studies. With Eq. (6), we have

$$\frac{1}{m}=n'+\frac{\sigma V}{\sqrt{3}k_BT}\,. \tag{7}$$

Eq.(7) shows the relationship among the strain rate sensitivity *m*, athermal stress exponent *n'*, and activation volume *V*. Only when the ratio of mechanical work over the thermal energy approaches zero, i.e., $\frac{\sigma V}{\sqrt{3}k_BT}\to 0$, we shall have $\frac{1}{m}=n'$. Eq. (7) also indicates that if the value of $\frac{\sigma V}{\sqrt{3}k_BT}$ is large and positive, the *m* value is still positive even the value *n'* is negative (Yang et al., 2016a; Yang et al., 2016b). Using the multi-temperature approach, the present work is going to verify that Eqs. (6) and (7) basically work for indentation creep.

3. Experimental Procedures

The presently used nt-Cu sheets are the same as previously used ones (Yang et al., 2016a;

Yang et al., 2016b), which were synthesized by direct current electro-deposition method with $CuSO_4$ electrolyte (Wang et al., 2009c; Xu et al., 2008). The transmission electron microscopy (TEM, JEOL 2010F) was operated at 200 kV to characterize the microstructure of nt-Cu before and after indentation creep tests. Fig. 1(a) is a TEM image of the used nt-Cu, showing intragranular nanotwins embedded ultrafine grains, which gives the average subgrain size of ~ 65 nm and the twin lamellar thickness of ~ 50 nm (Yang et al., 2016a; Yang et al., 2016b). The micro-indentation creep samples were polished with SiC paper from #600 to #1200, and finally 0.1 μm alumina suspensions. The micro-indentation creep tests were carried out with a NanoTest platform (Micro Materials Ltd, UK) equipped with a temperature stage and a Berkovich diamond indenter (the nominal tip radius of curvature is ~ 150 nm). The purpose of the present work is to study the indentation creep behavior of the nt-Cu specimens and thus the purely temperature-induced microstructure change of grain and twin growths should be avoided. The annealing experiment shows that the grain growth occurs in ng-Cu once the temperature is higher than 100 °C (Cai et al., 2000). To make sure there is no grain growth induced purely by the elevated temperature during the creep tests, therefore, the micro-indentation creep tests were isothermally conducted at various temperatures of RT, 40 ℃, 50 ℃, 60 ℃ and 70 ℃, which are all lower than the temperature of 100 °C. Fig. 1(b) provides the TEM image of the overall microstructure of the nt-Cu after the creep tests at temperature of 70 ℃, showing almost the same subgrain size and the twin lamellar thickness, comparing to that in the as-deposited nt-Cu without creep test in Fig. 1(a). This comparison implies that the thermal-induced grain growth and twin growth are not detected after the creep tests. Thermal drift is the most obvious problem in the nano/microindentation tests at elevated temperatures, especially for performing long-term creep tests at elevated temperatures. In the present work, the micro-indentation machine was well stabilized to minimize the thermal drift

lower than 0.01 nm/s and the temperature was precisely controlled with the error of ±0.1℃. Each isothermal micro-indentation creep test was repeated at least 5 times. Fig. 1(c) shows the morphology of one representative micro-indentation in the indented sample, where a Berkovich indenter-shaped plastic deformation region covers numbers of nanograins and nt lamellas. Following the multi-temperature approach, micro-indentation creep tests were performed at five temperatures of RT, 40 ℃, 50 ℃, 60 ℃ and 70 ℃ in the present study. The loading/unloading rates were set to be the same 2 mN/s for the five temperatures and the maximum sustained load was set at 100 mN to be the same for the five temperatures. Fig. 2(a) shows the load-time profile of the micro-indentation creep test at temperature of RT, where the load and indentation displacement are recorded as a function of indentation time. A load cell and a displacement voltage dilatometer with resolution of 0.1 nm and 100 nN, respectively, were used to control the applied load and to measure the penetration depth of the indenter. The indentation depth was controlled below 1/10 of the film thickness to avoid any potential substrate effect. Under a loading rate of 2 mN/s, the indentation load was increased from zero to a maximum load of 100 mN, which was fixed and hold for 1000 seconds (s) for the creep deformation, and then unloaded to zero with the unloading rate of 2 mN/s. The measurable indentation creep is observed, as shown in Fig. 2(a), with the creep displacement (indentation depth) increases within the entire creep time of 1000 s.

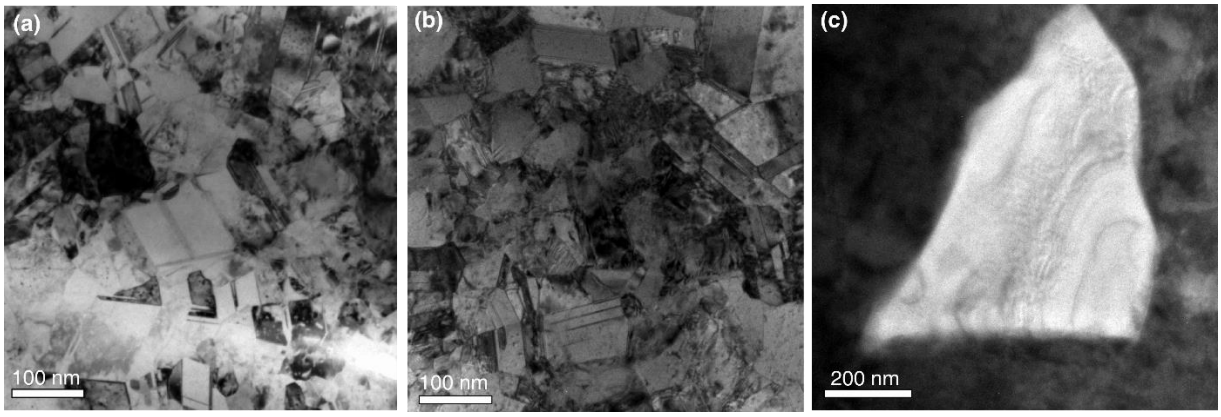

Figure 1 TEM images showing the microstructures of the **(a)** as-deposited, **(b)** as-crept nt-Cu at elevated temperature of 70 ºC, and **(c)** the morphology of one representative micro-indentation in the indented nt-Cu.

4. Results and Discussion

Note that it takes 50 s for the indentation load to increase from zero to the pre-set maximum sustained load, as the loading profile indicated in Fig. 2(a). Fig. 2(b) gives the indentation displacement h with the indentation time t from 50 s to 1050 s of the nt-Cu under sustained indentation load of 100 mN at various temperatures, where t = 50 s denotes the indentation creep starting time. The indentation creep is observed and measured at each of the five testing temperatures, as shown in Fig. 2(b). The indentation creep displacement increases monotonously as a function of the indentation time during the entire creep time. In particular, the starting indentation creep displacement at t = 50 s and the ending indentation creep displacement at t = 1050 s are respectively increased with the increase of the creep testing temperature. For example, at the creep time of 50 s, the corresponded starting indentation creep displacement is ~ 1430 nm at temperature of RT, which is increased to ~ 1520 nm at temperature of 70 ºC. On the other hand, the ending indentation creep displacement at the creep time of 1050 s are ~ 1620 nm at temperature of RT and ~ 2170 nm at temperature of 70 ºC. Accordingly, Fig. 2(c) shows the magnitude of total indentation creep displacement Δh as a function of creep time $\Delta t = t$ - 50 s, indicating the primary stage and the steady stage of creep. At a given creep time, the higher the creep temperature is, the larger the magnitude of indentation creep displacement will be. For example, when the indentation creep test last about 1000 s, the total indentation creep displacements are ~ 190 nm and ~ 650 nm at RT and 70 ℃, respectively. This phenomenon is expected since creep is a thermally activated process and can be promoted under a higher temperature.

For a self-similar indenter, generally, the hardness H and the indentation strain rate $\dot{\varepsilon}$ in the

displacement sensing indentation are respectively defined by (Lucas and Oliver, 1999; Mayo and Nix, 1988)

$$H = \frac{P}{A}, \tag{8a}$$

$$\dot{\varepsilon} = \frac{1}{h}\frac{dh}{dt}, \tag{8b}$$

where h is the instantaneous indenter displacement, dh/dt is the displacement rate of the indenter, with t being the creep time, P is the sustained creep load, and A is the projected contact area, which is estimated from indentation displacement h by

$$A = 24.56h^2 \tag{8c}$$

for the Berkovich indenter tip (Chang et al., 2006; Giannakopoulos and Suresh, 1999; Oliver and Pharr, 1992; Wang et al., 2013a; Zhang et al., 2017a).

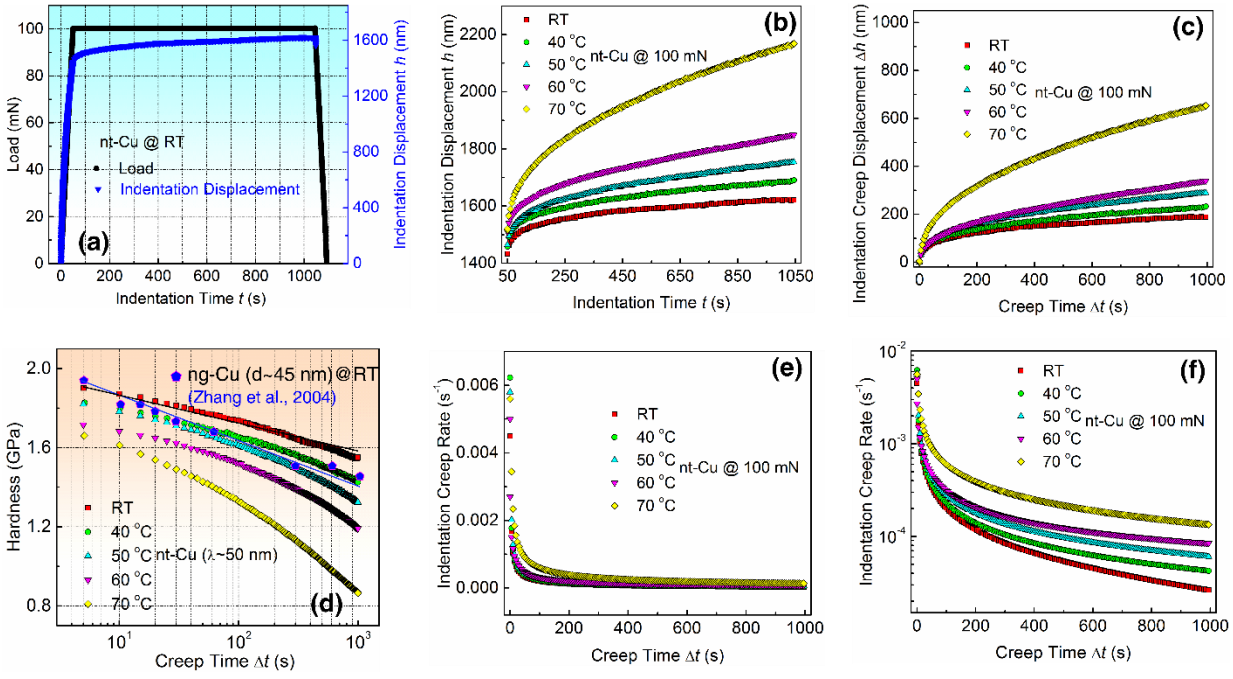

Figure 2 (a) The loading profile of the micro-indentation creep on the nt-Cu at RT. **(b)** The curves of the indentation displacement h with the indentation time t from 50 s to 1050 s of the nt-Cu at

various temperatures. **(c)** The magnitude of total indentation creep displacement Δh as a function of creep time Δt. **(d)** The curves of creep hardness versus logarithmic creep time, and **(e, f)** the curves of indentation creep rate **(e)**, and logarithmic indentation creep rate **(f)**, respectively, versus creep time under sustained load of 100 mN at various temperatures.

With Eq. (8a) and the measured data of creep depth versus creep time, the curves of creep hardness versus logarithmic creep time are plotted in Fig. 2(d) for the nt-Cu at various temperatures. The indentation creep hardness is apparently time- and temperature-dependent. At each of the creep temperatures, the hardness reduces monotonically with creep time. At a given creep time, the higher the creep temperature is, the lower the magnitude of hardness will be and the higher the reduction rate of hardness will be. Specifically, Fig. 2(d) also compare the reduction rate of hardness at RT in the nt-Cu to that in the twin-free ng-Cu with grain size of $d \sim 45$ nm from the reference (Zhang et al., 2004), because its grain size is slightly smaller than the twin lamellar thickness of $\lambda \sim 50$ nm in the nt-Cu. At the initial stage of the creep at RT, the hardness is ~1.9 GPa in the nt-Cu and ~ 1.95 GPa in the referenced ng-Cu, as shown in Fig. 2(d), which are correspondingly reduced to ~ 1.55 GPa and ~ 1.45 GPa after the creep tests last about 1000s. The averaged reduction rate of hardness of nt-Cu is 0.35 MPa/s, lower than that of 0.5 MPa/s in the reference ng-Cu. Considering the coherent nature of CTBs and the present results, one might believe that nt metals possess higher creep resistance and structural stability compared to their twin-free ng counterparts, i.e., the grain size in the ng counterparts should be more or less the same as the lamellar thickness in the nt metals. With Eq. (8b) and the measured data of creep displacement versus creep time, the curves of indentation creep rate versus creep time and logarithmic indentation creep rate versus creep time are respectively plotted in Fig. 2(e) and Fig. 2(f) at creep temperatures from RT to 70 ℃. At a given creep time, the creep rate increases obviously with the increase of the creep temperature. At each of the creep temperatures, the creep rate decreases continuously with the creep time, exhibiting two characteristic stages. It is noted that

creep rate decreases rapidly in the beginning and reaches an apparent steady state with a creep rate on the order of about 10^{-4} s^{-1}. The transient time from the primary to steady-state creep, or the primary creep region, is observed to increase with the test temperature. In the beginning stage, the creep rates drop very rapidly with creep time and after that the creep rates drop much more slowly. Taking the creep at 70 ℃ as an example, the creep rate decreases from ~ 5.6× 10^{-3} s^{-1} at t=0 to ~ 3.9 × 10^{-4} s^{-1} at t=200 s, and within the range of creep time (0s, 50s), the logarithmic indentation creep rate drops almost linearly with creep time with an absolute slope of ~ 9.5 × 10^{-5} s^{-2}. From t=200 s to t=1000 s, the creep rate falls from ~ 3.9 × 10^{-4} s^{-1} to 1.34× 10^{-4} s^{-1} roughly linearly with an absolute slope of ~ 3.7 × 10^{-7} s^{-2}, which is obviously lower in magnitude than that in the beginning stage. The difference in creep rate drop might imply the change in creep mechanism, which will be discussed later. The overall experimental results shown in Fig. 2(b-f) indicate clearly that, after a given indentation creep period, the higher the creep temperature is, the larger the indentation creep displacement Δh and the greater the hardness decreases, which implies that the creep rate during the same creep period increases with the creep temperature. In one sentence, the indentation creep deformation on nt-Cu is obviously accelerated with the increase of the indentation creep temperature.

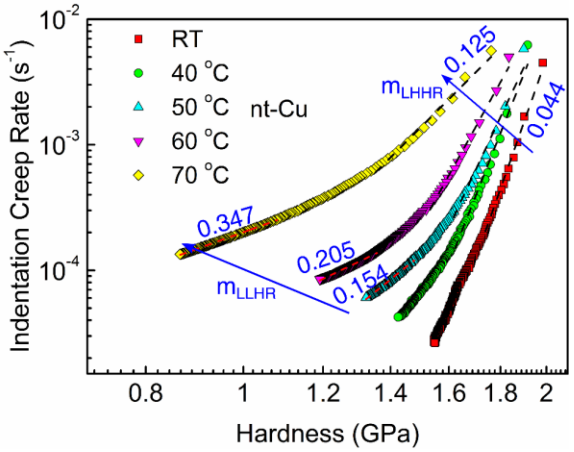

Figure 3 Plots of logarithmic indentation creep rate versus logarithmic hardness for the indentation creep of nt-Cu at various temperatures.

In analogy with Eq. (1), the strain rate sensitivity parameter m in the indentation creep may be defined by $m = \left.\frac{\partial \ln H}{\partial \ln \dot{\varepsilon}}\right|_T$. Fig. 3 plots the curves of logarithmic creep rate versus logarithmic hardness at various temperatures, showing that these curves can be approximately divided into two linear regions, i.e., the linear high hardness region (LHHR) in the initial stage and linear low hardness region (LLHR) in the final stage of indentation creep. The LHHR occurs at all the creep temperatures and at each of the temperatures, the logarithmic creep rate drops quickly with the decrease of logarithmic hardness. The higher the indentation creep temperature is, the lower the drop rate is and the shorter the LHHR is. The second LLHR happens with low hardness only at temperatures of 50 ^{o}C, 60 ^{o}C and 70 ^{o}C, showing that an apparently slower drop occurs in the logarithmic creep rate against logarithmic hardness. In LLHR, the lower the indentation creep temperature is, the faster the drop rate is, and the shorter the LLHR. Specifically, if the testing temperature is too low, the second LLHR will not show up at temperatures of RT and 40 ^{o}C, as indicated in Fig. 3, which implies that the indentation creep behaviors depend greatly on the testing temperature. The plastic deformation in indentation creep is attributed to the combined mechanical and thermal action, where hardness is still the driving force and the indentation creep is a thermally activated time-dependent process. Each slope of LHHR and LLHR denotes the strain rate sensitivity in that linear region. The determined values of m_{LHHR} in the first LHHR are 0.044, 0.049, 0.059, 0.069, and 0.125, respectively, at temperatures of RT, 40 ℃, 50 ℃, 60 ℃, and 70 ℃, while, the values of m_{LLHR} in the LLHR are 0.154 at 50 ℃, 0.205 at 60 ℃, and 0.347 at 70 ℃, higher than the corresponding values of m_{LHHR}, 0.059 at 50 ℃, 0.069 at 60 ℃, and 0.125 at 70 ℃, respectively.

The *m* parameter in each of the two linear regions depends highly on the temperature, that is, the higher the creep temperature is, the higher the strain rate sensitivity will be, as indicated in Fig.3. As indicated by the definition of Eq. (1), the value of strain rate sensitivity *m*, which represents the isothermal relationship between stress (hardness) and strain rate, is actually equal to the reciprocal of the conventional stress (hardness) exponent *n*, i.e., $m = 1/n$. Generally, a highly strain rate sensitive [or low conventional stress exponent] material is expected to resist localized deformation and hence be ductile, and even superplastic (Hutchinson and Neale, 1977), which is related to the diffusion-dominated creep mechanism. While the dislocation-mediated plasticity mechanism results in a low strain rate sensitivity [or highly conventional stress exponent]. The values of stress exponent ranging from 1 to 5 [or $0.2 < m < 1$] are widely reported for the creep deformation in various types of materials in many textbooks. According to the results shown in Fig. 3, the determined convention hardness exponents [or strain rate sensitivity] are $2.88 < n < 6.5$ [or $0.154 < m < 0.347$] in the LLHR, while $8 < n < 22.7$ [or $0.044 < m < 0.125$] in the LHHR with higher hardness level. Apparently, the values of conventional stress exponent *n* in the LHHR are higher than the typical values in the textbooks. This is because of that, besides the creep temperature, the strain rate sensitivity *m* (or the conventional stress exponent *n*) is also highly depended on the external stress/hardness condition (Liu et al., 2012). As the testing temperature is relative low and the applied stress (i.e., hardness) in the LHHR is much higher than the applied stress (normally lower than the yield strength) in the conventional creep tests reported in the textbooks, it might be reasonable to expect that a higher value of the conventional hardness exponent *n* would be observed in our experiments. In addition, it has been reported that the high value of *n* might be attributed to the volumetric densification and dislocation pile-up related creep mechanisms (Gan and Tomar, 2010; Gan et al., 2014). Furthermore, the value of the strain rate sensitivity parameter *m* [or

conventional stress exponent *n*] is depended on the material microstructure, and has been found to be increased commonly for fcc metals, with decreasing in the characteristic of grain size or twin spacing. For example, experiments have revealed that the *m* values of *m* = 0.01-0.03 in ultrafine grained metals, and *m* = 0.02-0.1 in ng and nt metals, which are higher than the values of *m* = 0.002-0.007 in the cg counterparts (Chen et al., 2006; Dalla Torre et al., 2002; Lu et al., 2001; Lu et al., 2005; Wei et al., 2004). The present experimental investigation measures the values of the strain rate sensitivity in the nt-Cu at the five temperatures. These values will be used to discuss the creep mechanism in the following section.

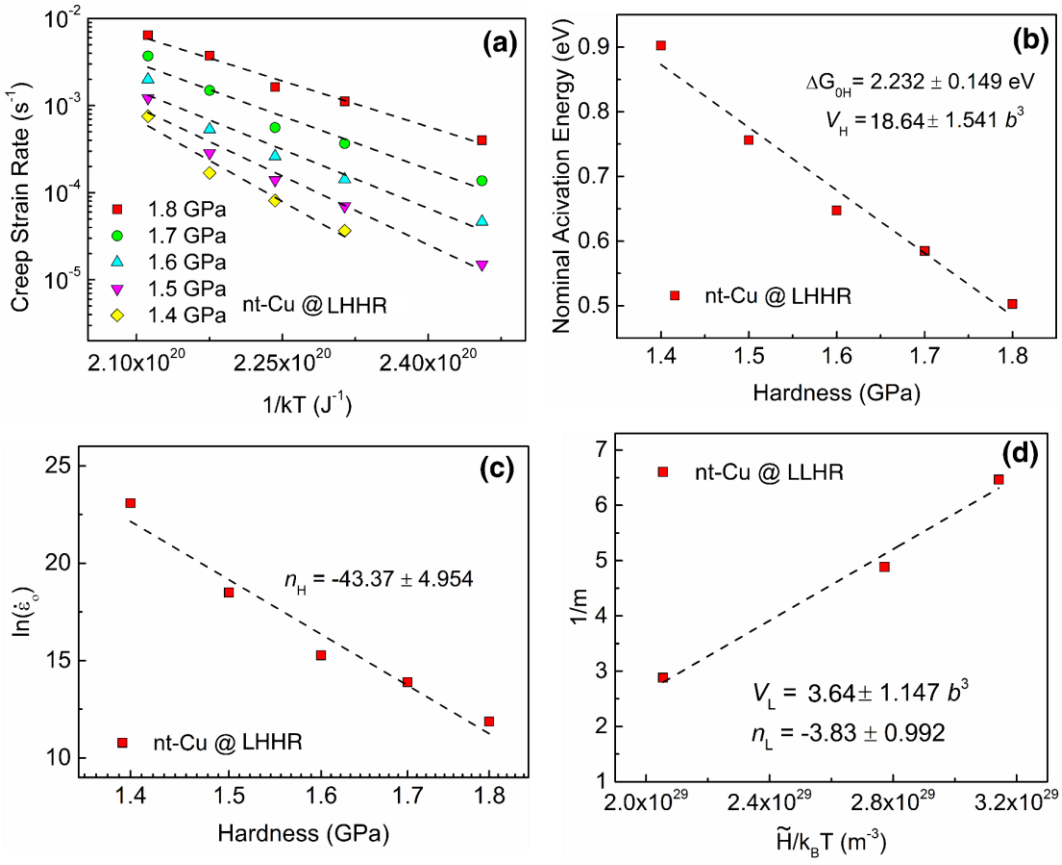

Figure 4 The determination of the thermal creep activation parameters in the two linear hardness regions for the nt-Cu. **(a)** Arrhenius plots of logarithmic indentation creep rate against the reciprocal temperature in the LHHR. **(b)** The plots of hardness-dependent nominal activation energy versus hardness in the LHHR. **(c)** The plots of logarithmic temperature-independent creep

rate versus logarithmic hardness in the LHHR. **(d)** The reciprocal strain rate sensitivity against the term of $\tilde{H}/k_BT$ at various temperatures in the LLHR.

In nano/micro-indentation, hardness H is actually the averaged compressive stress, as shown by Eq. (8a), on the projected contact area. The value of hardness is automatically and instantly determined by the computerized indentation machine. In analogy with Eq. (2) in the Arrhenius relation, the creep rate in indentation creep might be expressed by replacing stress with hardness,

$$\dot{\varepsilon}(H,T)=\dot{\varepsilon}_0(H)\exp\left(-\frac{\Delta G}{k_BT}\right), \tag{9a}$$

where $\dot{\varepsilon}_0(H)$ and ΔG are the prefactor and the apparent (nominal) activation energy. Again, the hypothesis holds in Eq. (9a), meaning that the prefactor and the apparent activation energy are temperature-independent and depend on hardness. The apparent activation energy ΔG and the logarithmic prefactor $\ln\left(\dot{\varepsilon}_0(H)\right)$ can be determined from the Arrhenius plots of logarithmic creep rate at the same hardness level against reciprocal temperature.

As described in the previous section and shown in the Fig. 2 (c-d) and Fig. 3, the hardness and the creep rate in the indentation creep are reduced with the increase of creep time at each of the temperatures and there are two linear regions of LHHR and LLHR. Note that a sustained load in indentation creep tests generates various values of hardness, meaning that the varying the value of hardness is achieved by changing temperature, even the applied load remains unchanged. Therefore, a series of these two hardness-dependent activation parameters can be obtained from Arrhenius plots under a series of hardness in the indentation creep tests performed under only one sustained load. This is different from that in the uniaxial tensile or compressive creep experiments, where the varying the level of applied stress requires to change the magnitude of applied load when the

sample geometry and size remain unchanged. Fig. 4(a) gives the Arrhenius plots of the logarithmic creep strain rate versus reciprocal temperature under a series of hardness of 1.4 GPa, 1.5 GPa, 1.6 GPa, 1.7 GPa, and 1.8 GPa in the LHHR shown in Fig. 3. The experimental data are selected to cover, as many as possible, the five creep temperatures. As shown in Fig. 4(a), the data for hardness 1.4 GPa covers four temperatures and the rest data cover all the five temperatures. As expected, Fig 4(a) shows that the curves of the logarithmic strain rate versus reciprocal temperature are almost linear under a given hardness, indicating that the indentation creep is thermally activated deformation and the creep rate follows the Arrhenius relation of Eq. (9a) over the testing temperature range. The experimental results confirm the hypothesis again. The slope of the linear fitting of the experimental data under a given hardness gives the value of the apparent activation energy ΔG, while the fitted intercept determines the logarithmic temperature-independent creep rate $\ln\left(\dot{\varepsilon}_0(H)\right)$.

The apparent activation energy denotes real energy barrier, reduced by applied stress (hardness), to against the dislocation motion, GB and TB movement, or/and diffusion, etc. The activation volume, as a thermodynamic conjugate of flow stress, represents the generalized change in volume caused by flow stress and the mechanical work, e.g., the product of activation volume and flow stress, can reduce the activation energy. In dislocation-mediated deformation, the activation volume represents the generalized area swept over by mobile dislocations with an averaged value of Burgers vector. In indentation creep, hardness represents the averaged applied compressive stress on the projective contact area. Thus, a common and simple relationship between the apparent activation energy, hardness and activation volume can be expressed by

$$\Delta G = \Delta G_0 - H\tilde{V} = \Delta G_0 - \frac{H}{2}V, \tag{9b}$$

where ΔG_0 is a hardness-independent intrinsic activation energy or activation energy at zero of hardness, $\tilde{V}$ is called the hardness conjugated activation volume, the half is approximately introduced to link hardness to the maximum shear stress based on the elastic Hertz contact theory (Johnson, 1985), and V is the shear stress conjugated activation volume. The determined nominal activation energy in the LHHR is plotted versus the hardness in Fig. 4(b), showing that the nominal activation energy decreases almost linearly with increasing hardness, which verifies that Eq. (9b) holds. Based on Eq. (9b), the linearly fitting the curves of apparent activation energy versus hardness determines the ΔG_0 and V to be $\Delta G_{0\mathrm{H}}$ = 2.232 eV and V_{H} = 18.64 b^3 in the LHHR, respectively, with b = 2.56 Å standing for the magnitude of Burgers vector of a perfect dislocation $\frac{1}{2}\langle\bar{1}10\rangle\{111\}$ in fcc copper.

On the other hand, Fig. 4(c) shows an almost linear relationship between the $\ln\left(\dot{\varepsilon}_0(H)\right)$ versus logarithmic hardness in the LHHR, indicating that the prefactor, i.e., temperature-independent plastic deformation rate, depends on hardness with a power law relation, which is expressed by

$$\dot{\varepsilon}_0(H) = \dot{\varepsilon}_{00}\left(\frac{H}{H_0}\right)^{n'}, \tag{9c}$$

where $\dot{\varepsilon}_{00}$ and H_0 are the hardness-independent parameter and reference hardness, respectively; while n' is the athermal hardness exponent for the temperature-independent indentation creep rate component/prefacor $\dot{\varepsilon}_0(H)$ in the Eq. (9a). Note that the strain rate sensitivity is determined from the linearly fitting of the experimental data curves of log-log plots of creep rate versus hardness, as shown in Fig. 3. Therefore, the athermal hardness exponent n' in the present work is actually different from the traditional "stress exponent n", i.e., 1/m, for the creep strain rate in the conventional creep research community. Linear fitting of the experimental data of $\ln\left(\dot{\varepsilon}_0(H)\right)$

versus logarithmic hardness yields the athermal hardness exponent of n'_{H} = -43.37 in the LHHR. Noticeably, the athermal hardness exponent n' is negative here, which will be discussed later. Substituting Eqs. (9b-9c) into Eq. (9a), the Arrhenius equation for the indentation creep can be finally re-written as:

$$\dot{\varepsilon}(H,T) = \dot{\varepsilon}_{00}\left(\frac{H}{H_0}\right)^{n'} \exp\left(-\frac{\Delta G_0}{k_B T} + \frac{HV}{2k_B T}\right) \tag{9d}$$

Eq. (9d) is the experimentally verified strain rate equation with hardness and temperature as independent parameters for indentation creep. From Eq. (9d), we have

$$\frac{1}{m} = n' + \frac{HV}{2k_{\mathrm{B}}T} \tag{10}$$

for the relationship between the parameters of the strain rate sensitivity m, athermal hardness exponent n' and activation volume V. Eq. (10) is obviously the version of Eq. (6) for indentation creep. This relationship indicates the $1/m$ change linearly with hardness. As described above and in the previous works (Yang et al., 2016a; Yang et al., 2016b), experimental errors and the small variation in hardness keep the m value approximately constant in a narrow hardness range. With this approximation, we may write $\frac{1}{m} = n' + \frac{\tilde{H}V}{2k_{\mathrm{B}}T}$, where $\tilde{H}$ is the average hardness in the LHHR. The experimentally determined value of the $1/m$, n', the calculated term of $\frac{\tilde{H}V}{2k_B T}$, and the average hardness $\tilde{H}$ in the LHHR at various temperatures are listed in Table. 1 and these data validate the relationship of $\frac{1}{m} = n' + \frac{\tilde{H}V}{2k_{\mathrm{B}}T}$. For instance, it has $\frac{1}{m}(8.016) \approx n'(-43.37) + \left.\frac{\tilde{H}V}{2k_B T}\right|_{70\,^{\circ}\mathrm{C}} (51.313)$ with average hardness $\tilde{H}$ of 1.562 GPa in the LHHR at 70 ℃. As indicated in Fig. 3, no LLHR shows up at temperatures of RT and 40 ºC and it is very hard to find three data with the same value

of hardness at three temperatures in the LLHRs, while a reasonable Arrhenius plot of logarithmic creep strain rate versus reciprocal temperature requires at least three data. The experimental data in the LLHRs do not meet the requirement of the multi-temperature approach. Therefore, the apparent activation energy at a given hardness cannot be determined in the LLHRs. Fortunately, three values of m are determined from the experimental data shown in Fig. 3, which allows to plot the reciprocal strain rate sensitivity $1/m$ against the term of $\frac{\tilde{H}}{k_B T}$ in Fig. 4(d) with $\tilde{H}$ being the average hardness within a given LLHR based on the relationship of $\frac{1}{m} = n' + \frac{\tilde{H}V}{2k_B T}\Big|_T$. Fig. 4(d) shows an almost linear relationship and the linear fitting gives the values of activation volume V and athermal hardness exponent n', which are $V_L = 3.64\ b^3$ and athermal hardness exponent $n'_L = -3.83$ in the LLHRs.

Table 1 The determined reciprocal strain rate sensitivity m, athermal hardness exponent n', the term $\frac{\tilde{H}V}{2k_B T}$, and the average hardness $\tilde{H}$ in the LHHRs.

	Linear High Hardness Region (LHHR)				
	RT	40 ºC	50 ºC	60 ºC	70 ºC
m	0.044	0.049	0.059	0.069	0.125
$1/m$	22.726	20.286	17.080	14.491	8.016
n'	-43.37	-43.37	-43.37	-43.37	-43.37
$\frac{\tilde{H}V}{2k_B T}$	67.264	64.009	61.260	57.152	51.313
$\tilde{H}$ (GPa)	1.76	1.778	1.756	1.689	1.562

As described above, the athermal hardness exponent n' are both negative in the two linear hardness regions, meaning that the temperature-independent prefactor $\dot{\varepsilon}_0$ is decreased with the increase of hardness. As indicated by Eq. (9d), the hardness contribution to the creep strain rate is done through two channels, a) lowering the intrinsic activation energy by doing the mechanical work with its thermodynamic conjugate of activation volume, and b) changing the value of hardness-dependent prefactor $\dot{\varepsilon}_0$. While the temperature contribution to the creep rate is just done through one channel, i.e., increasing the thermal energy of k_BT in the exponential part in Eq. (9d), which will increase the strain rate exponentially, as evidenced by the experimental results of accelerated indentation creep deformation with the increase of temperature shown in Fig. 2.

The determined deformation parameters, i.e., strain rate sensitivity *m*, activation volume *V* and activation energy ΔG_0, might uncover the micro-indentation creep competing mechanisms in the two linear hardness regions. In the LHHR, the values of *m*, *V* and ΔG_0 are 0.044-0.125(RT-70 ℃), 18.64 b^3 and 2.323 eV, respectively, whereas the *m* is 0.154-0.347(50 ℃-70 ℃) and *V* is 3.64 b^3 in the LLHR. It has been widely accepted that a low *m* [high conventional stress exponent *n*] ($m < 0.1$, [$n > 10$]) (Coble, 1963; Lüthy et al., 1979), large *V* (several hundred b^3 and above) (Dao et al., 2006; Lu et al., 2005), and large ΔG_0 (ΔG_0>1 eV) (Wang et al., 2006) relate to the dislocation-mediated plasticity. While GB diffusion creep (Coble creep) results in the large *m* (m ~ 1.0, [$n \sim 1$]) (Coble, 1963; Lüthy et al., 1979), extreme small *V* (less than 1 b^3) (Dao et al., 2006; Lu et al., 2005) and ΔG_0 (0.2-0.7 eV) (Cai et al., 2000; Dickenscheid et al., 1991; Horváth et al., 1987; Van Swygenhoven and Caro, 1998). The $0.1 < m < 1$ [$1< n < 10$] might be related to the GB sliding or/and grain rotation. The *V* ranging from several b^3 to 100 b^3 might be corresponded to the dislocation cross-slip or/and dislocation nucleation (Dao et al., 2006; Lu et al., 2005; Wang et al.,

2011). Besides, the generalized swept area by dislocations can also be calculated according to the definition of activation volume. Assuming the perfect dislocation sweep mechanism applicable in all hardness regions, hence the swept area in the LHHR is 1.09 $(nm)^2$, referring to the GBs and TBs impede dislocation motion. However, it decreases to 0.21 $(nm)^2$ in the LLHR, which is too small to believe the perfect dislocation sweep mechanism, thus suggesting the GB/TB movement, or/and partial dislocation-mediated creep mechanisms. Combing all determined deformation parameters, we suggest the predominant indentation creep mechanism transition with the decrease of hardness, i.e., from the dislocation activity-dominated deformation in the LHHR primary creep region to the boundary-associated deformation in the LLHR steady-state creep region. The dislocation activity-dominated deformation might be attributed to the interaction of dislocations with the GBs and TBs in the nt-Cu, such as dislocation pile-up and cut-off the twin lamellas (Dao et al., 2006; Lu et al., 2005; Lu et al., 2009; Wang et al., 2012a; Yang et al., 2016a; Yang et al., 2016b). On the other hand, different from the GB sliding or/and grain rotation boundary-associated deformation in ng structure, the TB rotation is confined and difficult to occur as the twin planes are coherent in nature. Alternatively, the nucleation and motion of partial dislocations parallel to TBs, i.e., TB migration, could be the creep mechanism in the lower hardness region, which has been reported by simulations (Li et al., 2010) and observed by high-resolution TEM for the nt-Cu with the same order values of the deformation parameters in the previous works (Yang et al., 2016a; Yang et al., 2016b).

5. Concluding Remarks

In summary, the present work analyzes the mathematic inconsistency when the strain rate sensitivity m is used to express the stress exponent n and to estimate the activation volume V, simultaneously. The analysis indicates that multi-temperature approach must be adopted in order to determine the athermal stress exponent n' and the apparent activation energy, and then the

intrinsic activation energy and the activation volume. The multi-temperature indentation creep tests were conducted on nt-Cu, which generated a large number of experimental data. It is the experimental data driven development of the indentation creep formula that the strain rate is a function of temperature and hardness, which represents the mechanical loading level. The experimental results verify the developed formula, which is explicit, analytic, and user friendly. This formula is essentially based on the Arrhenius equation and the temperature dependency is purely via the exponential term, rather than via the prefactor. The intrinsic activation energy, apparent activation energy, and mechanical work are all independent of temperature within a certain temperature range during which no change in the deformation mechanism occurs. The athermal hardness exponent is introduced naturally to express the hardness dependency of the prefactor. The hardness contribution to the creep strain rate is attributed to two aspects, thermal and athermal, i.e., a) the reduction of the intrinsic activation energy by the mechanical work with its thermodynamic conjugate of activation volume and b) the change in the value of prefactor through a manner of power law. While, the temperature contribution to the creep rate is purely through the change of the exponential term by varying the thermal energy of k_BT. Equations (9d) and (10) represent the theoretical achievement of the present work.

The experimental data shows the greater indentation creep resistance of the nt-Cu compared to that of the reference twin-free ng counterpart. In addition, the indentation creep deformation on nt-Cu is obviously accelerated with the increase of the indentation creep temperature. The results of multi-temperature indentation creep tests also indicate the change in the strain rate sensitivity m at the testing temperatures of 50 ℃, 60 ℃ and 70 ℃, where the experimental curves of logarithmic indentation creep rate versus logarithmic creep hardness can be approximately divided into two linear regions of the linear high hardness region (LHHR) in the initial stage and the linear low

hardness region (LLHR) in the final stage of indentation creep. The change in the strain rate sensitivity *m* implies the change in the creep mechanism. Analysis on all determined values of the intrinsic parameters suggests a transition of indentation creep mechanism from perfect dislocation mediated plasticity in the LHHR to the twin boundary migration in the LLHR.

Acknowledgments

The present research is supported by the PolyU internal grants (No. 1-ZE8R and No. G-YBDH), NSFC (No. 51271157), the research grants (No. 15DZ2260300 and No. 16DZ2260600) from the Science and Technology Commission of Shanghai Municipality, and the 111 project (No. D16002) from the Ministry of Education and the State Administration of Foreign Experts Affairs, PRC. We also thank Prof. Guoyong Wang for his help in the sample preparation.

References:

Alizadeh, R., Mahmudi, R., Langdon, T.G., 2013. Creep mechanisms in an Mg–4Zn alloy in the as-cast and aged conditions. Mater. Sci. Eng. A 564, 423-430.

Asaro, R.J., Suresh, S., 2005. Mechanistic models for the activation volume and rate sensitivity in metals with nanocrystalline grains and nano-scale twins. Acta Mater. 53, 3369-3382.

Basirat, M., Shrestha, T., Potirniche, G.P., Charit, I., Rink, K., 2012. A study of the creep behavior of modified 9Cr–1Mo steel using continuum-damage modeling. Inter. J. Plasticity 37, 95-107.

Bezares, J., Jiao, S., Liu, Y., Bufford, D., Lu, L., Zhang, X., Kulkarni, Y., Asaro, R.J., 2012. Indentation of nanotwinned fcc metals: Implications for nanotwin stability. Acta Mater. 60, 4623-4635.

Cai, B., Kong, Q.P., Lu, L., Lu, K., 2000. Low temperature creep of nanocrystalline pure copper. Mater. Sci. Eng. A 286, 188-192.

Cao, Z.H., Wang, L., Hu, K., Huang, Y.L., Meng, X.K., 2012. Microstructural evolution and its influence on creep and stress relaxation in nanocrystalline Ni. Acta Mater. 60, 6742-6754.

Chang, S.-Y., Lee, Y.-S., Chang, T.-K., 2006. Nanomechanical response and creep behavior of electroless deposited copper films under nanoindentation test. Mater. Sci. Eng. A 423, 52-56.

Chen, J., Lu, L., Lu, K., 2006. Hardness and strain rate sensitivity of nanocrystalline Cu. Scr. Mater. 54, 1913-1918.

Choi, I.-C., Kim, Y.-J., Seok, M.-Y., Yoo, B.-G., Kim, J.-Y., Wang, Y., Jang, J.-i., 2013a. Nanoscale room temperature creep of nanocrystalline nickel pillars at low stresses. Inter. J. Plasticity 41, 53-64.

Choi, I.-C., Kim, Y.-J., Wang, Y.M., Ramamurty, U., Jang, J.-i., 2013b. Nanoindentation behavior of nanotwinned Cu: Influence of indenter angle on hardness, strain rate sensitivity and activation volume. Acta Mater. 61, 7313-7323.

Coble, R.L., 1963. A Model for Boundary Diffusion Controlled Creep in Polycrystalline Materials. J. Appl. Phys. 34, 1679-1682.

Dalla Torre, F., Van Swygenhoven, H., Victoria, M., 2002. Nanocrystalline electrodeposited Ni: microstructure and tensile properties. Acta Mater. 50, 3957-3970.

Dao, M., Lu, L., Shen, Y.F., Suresh, S., 2006. Strength, strain-rate sensitivity and ductility of copper with nanoscale twins. Acta Mater. 54, 5421-5432.

Dickenscheid, W., Birringer, R., Gleiter, H., Kanert, O., Michel, B., Günther, B., 1991. Investigation of self-diffusion in nanocrystalline copper by NMR. Solid State Commun. 79, 683-686.

Dieter, G.E., 1986. Mechanical metallurgy. (3rd ed.)McGraw-Hill, Boston (MA).

Elmustafa, A.A., Stone, D.S., 2002. Indentation size effect in polycrystalline F.C.C. metals. Acta Mater. 50, 3641-3650.

Fischer, F.D., Svoboda, J., 2011. Chemically and mechanically driven creep due to generation and annihilation of vacancies with non-ideal sources and sinks. Inter. J. Plasticity 27, 1384-1390.

Gan, M., Tomar, V., 2010. Role of length scale and temperature in indentation induced creep behavior of polymer derived Si–C–O ceramics. Mater. Sci. Eng. A 527, 7615-7623.

Gan, M., Tomar, V., 2011. Scale and temperature dependent creep modeling and experiments in materials. Jom 63, 27.

Gan, M., Zhang, Y., Tomar, V., 2014. In Situ Deformation of Silicon Cantilever Under Constant Stress as a Function of Temperature. J. Nanotechnol. Eng. Med. 5, 021004 021001-021009.

Giannakopoulos, A.E., Suresh, S., 1999. Determination of elastoplastic properties by instrumented sharp indentation. Scr. Mater. 40, 1191-1198.

He, B.B., Luo, H.W., Huang, M.X., 2016. Experimental investigation on a novel medium Mn steel combining transformation-induced plasticity and twinning-induced plasticity effects. Inter. J. Plasticity 78, 173-186.

Herring, C., 1950. Diffusional Viscosity of a Polycrystalline Solid. J. Appl. Phys. 21, 437-445.

Horváth, J., Birringer, R., Gleiter, H., 1987. Diffusion in nanocrystalline material. Solid State Commun. 62, 319-322.

Hutchinson, J., Neale, K., 1977. Influence of strain-rate sensitivity on necking under uniaxial tension. Acta Metall. 25, 839-846.

Jia, Y., Peng, K., Gong, X.-l., Zhang, Z., 2011. Creep and recovery of polypropylene/carbon nanotube composites. Inter. J. Plasticity 27, 1239-1251.

Jiao, S., Kulkarni, Y., 2015. Molecular dynamics study of creep mechanisms in nanotwinned metals. Comput. Mater. Sci. 110, 254-260.

Johnson, K.L., 1985. Contact Mechanics. Cambridge University Press, Cambridge.

Kassner, M.E., Kumar, P., Blum, W., 2007. Harper–Dorn creep. Inter. J. Plasticity 23, 980-1000.

Kassner, M.E., Pérez-Prado, M.T., 2004. Fundamentals of Creep in Metals and Alloys. Elsevier Science Ltd, Oxford.

Lee, D.-H., Seok, M.-Y., Zhao, Y., Choi, I.-C., He, J., Lu, Z., Suh, J.-Y., Ramamurty, U., Kawasaki, M., Langdon, T.G., Jang, J.-i., 2016. Spherical nanoindentation creep behavior of nanocrystalline and coarse-grained CoCrFeMnNi high-entropy alloys. Acta Mater. 109, 314-322.

Li, X., Dao, M., Eberl, C., Hodge, A.M., Gao, H., 2016. Fracture, fatigue, and creep of nanotwinned metals. MRS Bull. 41, 298-304.

Li, X., Wei, Y., Lu, L., Lu, K., Gao, H., 2010. Dislocation nucleation governed softening and maximum strength in nano-twinned metals. Nature 464, 877-880.

Liu, Y., Huang, C., Bei, H., He, X., Hu, W., 2012. Room temperature nanoindentation creep of nanocrystalline Cu and Cu alloys. Mater. Lett. 70, 26-29.

Lu, L., Li, S.X., Lu, K., 2001. An abnormal strain rate effect on tensile behavior in nanocrystalline copper. Scr. Mater. 45, 1163-1169.

Lu, L., Schwaiger, R., Shan, Z.W., Dao, M., Lu, K., Suresh, S., 2005. Nano-sized twins induce high rate sensitivity of flow stress in pure copper. Acta Mater. 53, 2169-2179.

Lu, L., Shen, Y., Chen, X., Qian, L., Lu, K., 2004. Ultrahigh Strength and High Electrical Conductivity in Copper. Science 304, 422-426.

Lu, L., Zhu, T., Shen, Y., Dao, M., Lu, K., Suresh, S., 2009. Stress relaxation and the structure size-dependence of plastic deformation in nanotwinned copper. Acta Mater. 57, 5165-5173.

Lucas, B., Oliver, W., 1999. Indentation power-law creep of high-purity indium. Metall. Mater. Tran. A 30, 601-610.

Lüthy, H., White, R.A., Sherby, O.D., 1979. Grain boundary sliding and deformation mechanism maps. Mater. Sci. Eng. A 39, 211-216.

Ma, Z.S., Zhou, Y.C., Long, S.G., Lu, C., 2012. On the intrinsic hardness of a metallic film/substrate system: Indentation size and substrate effects. Inter. J. Plasticity 34, 1-11.

Ma, Z.Y., Mishra, R.S., Tjong, S.C., 2002. High-temperature creep behavior of TiC particulate reinforced Ti–6Al–4V alloy composite. Acta Mater. 50, 4293-4302.

Mayo, M.J., Nix, W.D., 1988. A micro-indentation study of superplasticity in Pb, Sn, and Sn-38 wt% Pb. Acta Metall. 36, 2183-2192.

Morra, P.V., Radelaar, S., Yandouzi, M., Chen, J., Böttger, A.J., 2009. Precipitate coarsening-induced plasticity: Low temperature creep behaviour of tempered SAE 52100. Inter. J. Plasticity 25, 2331-2348.

Muñoz-Morris, M.A., Gutierrez-Urrutia, I., Morris, D.G., 2009. Influence of nanoprecipitates on the creep strength and ductility of a Fe–Ni–Al alloy. Inter. J. Plasticity 25, 1011-1023.

Oberson, P.G., Ankem, S., 2009. The effect of time-dependent twinning on low temperature ($<0.25*Tm$) creep of an alpha-titanium alloy. Inter. J. Plasticity 25, 881-900.

Oliver, W.C., Pharr, G.M., 1992. An improved technique for determining hardness and elastic modulus using load and displacement sensing indentation experiments. J. Mater. Res. 7, 1564-1583.

Raj, S.V., Langdon, T.G., 1989. Creep behavior of copper at intermediate temperatures-I. Mechanical characteristics. Acta Metall. 37, 843-852.

Ranganath, S., Mishra, R.S., 1996. Steady state creep behaviour of particulate-reinforced titanium matrix composites. Acta Mater. 44, 927-935.

Sanders, P.G., Fougere, G.E., Thompson, L.J., Eastman, J.A., Weertman, J.R., 1997. Improvements in the synthesis and compaction of nanocrystalline materials. Nanostruct. Mater. 8, 243-252.

Sharma, G., Ramanujan, R.V., Kutty, T.R.G., Prabhu, N., 2005. Indentation creep studies of iron aluminide intermetallic alloy. Intermetallics 13, 47-53.

Tehrani, M., Safdari, M., Al-Haik, M.S., 2011. Nanocharacterization of creep behavior of multiwall carbon nanotubes/epoxy nanocomposite. Inter. J. Plasticity 27, 887-901.

Van Swygenhoven, H., Caro, A., 1998. Plastic behavior of nanophase metals studied by molecular dynamics. Phys. Rev. B 58, 11246-11251.

Wang, B., Idrissi, H., Galceran, M., Colla, M.S., Turner, S., Hui, S., Raskin, J.P., Pardoen, T., Godet, S., Schryvers, D., 2012a. Advanced TEM investigation of the plasticity mechanisms in nanocrystalline freestanding palladium films with nanoscale twins. Inter. J. Plasticity 37, 140-156.

Wang, C.L., Zhang, M., Nieh, T.G., 2009a. Nanoindentation creep of nanocrystalline nickel at elevated temperatures. J. Phys. D: Appl. Phys. 42, 115405.

Wang, F., Li, J.M., Huang, P., Wang, W.L., Lu, T.J., Xu, K.W., 2013a. Nanoscale creep deformation in Zr-based metallic glass. Intermetallics 38, 156-160.

Wang, G., Lian, J., Jiang, Z., Qin, L., Jiang, Q., 2009b. Compressive creep behavior of an electric brush-plated nanocrystalline Cu at room temperature. J. Appl. Phys. 106, 086105.

Wang, G.Y., Jiang, Z.H., Lian, J.S., Jiang, Q., 2009c. The grain refinement mechanism of electrodeposited copper. J. Mater. Res. 24, 3226-3236.

Wang, S., Ye, Y.F., Sun, B.A., Liu, C.T., Shi, S.Q., Yang, Y., 2015. Softening-induced plastic flow instability and indentation size effect in metallic glass. J. Mech. Phys. Solids 77, 70-85.

Wang, Y.-J., Gao, G.-J.J., Ogata, S., 2013b. Atomistic understanding of diffusion kinetics in nanocrystals from molecular dynamics simulations. Phys. Rev. B 88, 115413.

Wang, Y.-J., Ishii, A., Ogata, S., 2011. Transition of creep mechanism in nanocrystalline metals. Phys. Rev. B 84, 224102.

Wang, Y.-J., Ishii, A., Ogata, S., 2012b. Grain Size Dependence of Creep in Nanocrystalline Copper by Molecular Dynamics. Mater. Tran. 53, 156-160.

Wang, Y.M., Hamza, A.V., Ma, E., 2006. Temperature-dependent strain rate sensitivity and activation volume of nanocrystalline Ni. Acta Mater. 54, 2715-2726.

Wei, Q., Cheng, S., Ramesh, K.T., Ma, E., 2004. Effect of nanocrystalline and ultrafine grain sizes on the strain rate sensitivity and activation volume: fcc versus bcc metals. Mater. Sci. Eng. A 381, 71-79.

Xiao, X., Song, D., Chu, H., Xue, J., Duan, H., 2015. Mechanical behaviors of irradiated FCC polycrystals with nanotwins. Inter. J. Plasticity 74, 110-126.

Xu, L., Xu, D., Tu, K.N., Cai, Y., Wang, N., Dixit, P., Pang, J.H.L., Miao, J.M., 2008. Structure and migration of (112) step on (111) twin boundaries in nanocrystalline copper. J. Appl. Phys. 104, 5.

Yang, X.-S., Wang, Y.-J., Wang, G.-Y., Zhai, H.-R., Dai, L.H., Zhang, T.-Y., 2016a. Time, stress, and temperature-dependent deformation in nanostructured copper: Stress relaxation tests and simulations. Acta Mater. 108, 252-263.

Yang, X.-S., Wang, Y.-J., Zhai, H.-R., Wang, G.-Y., Su, Y.-J., Dai, L.H., Ogata, S., Zhang, T.-Y., 2016b. Time-, stress-, and temperature-dependent deformation in nanostructured copper: Creep tests and simulations. J. Mech. Phys. Solids 94, 191-206.

Zhang, X., Misra, A., 2012. Superior thermal stability of coherent twin boundaries in nanotwinned metals. Scr. Mater. 66, 860-865.

Zhang, X., Misra, A., Wang, H., Nastasi, M., Embury, J.D., Mitchell, T.E., Hoagland, R.G., Hirth, J.P., 2004. Nanoscale-twinning-induced strengthening in austenitic stainless steel thin films. Appl. Phys. Lett. 84, 1096-1098.

Zhang, Y., Mohanty, D.P., Seiler, P., Siegmund, T., Kruzic, J.J., Tomar, V., 2017a. High temperature indentation based property measurements of IN-617. Inter. J. Plasticity 96, 264-281.

Zhang, Y., Wang, H., Tomar, V., 2017b. Visualizing Stress and Temperature Distribution During Elevated Temperature Deformation of IN-617 Using Nanomechanical Raman Spectroscopy. Jom.

Zheng, S., Beyerlein, I.J., Carpenter, J.S., Kang, K., Wang, J., Han, W., Mara, N.A., 2013. High-strength and thermally stable bulk nanolayered composites due to twin-induced interfaces. Nat. Commun. 4, 1696.

Zhu, T., Li, J., 2010. Ultra-strength materials. Prog. Mater. Sci. 55, 710-757.

Zhu, T., Li, J., Samanta, A., Kim, H.G., Suresh, S., 2007. Interfacial plasticity governs strain rate sensitivity and ductility in nanostructured metals. Proc. Natl. Acad. Sci. U.S.A. 104, 3031-3036.